Influence of the crystallinity on the physicochemical properties of spray-dried quercetin-inulin microparticles and their performance during *in vitro* digestion

Alejandra Quintriqueo-Cid[1,4], Begoña Giménez[2], Patricio Romero-Hasler[1], Eduardo Soto-Bustamante[3], Jesús Lozano-Sánchez[4], Paz Robert[1]*

[1]Departamento de Ciencia de los Alimentos y Tecnología Química, Facultad de Ciencias Químicas y Farmacéuticas, Universidad de Chile, Dr. Carlos Lorca Tobar 964, Independencia, 81380494, Santiago, Chile. (A.Q.-C., aquintriqueo@ug.uchile.cl; P.R.-H., patricio.romero@ciq.uchile.cl).

[2]Departamento de Ciencia y Tecnología de los Alimentos, Facultad Tecnológica, Universidad de Santiago de Chile, Av. Victor Jara 3769, Estación Central, 9170124, Santiago, Chile. (B.G., bego.gimenez@usach.cl).

[3]Departamento de Química Orgánica y Fisicoquímica, Facultad de Ciencias Químicas y Farmacéuticas, Universidad de Chile, Dr. Carlos Lorca Tobar 964, Independencia, 81380494, Santiago, Chile. (E.S.-B., esoto@ciq.uchile.cl).

[4]Department of Food Science and Nutrition, Faculty of Pharmacy, University of Granada, Campus Universitario de Cartuja 1807, Granada, Spain. (J.L.-S., jesusls@ugr.es).

*Correspondence: Dra. Paz Robert, Facultad de Ciencias Químicas y Farmacéuticas, Departamento de Ciencia de los Alimentos y Tecnología Química, Universidad de Chile, Dr. Carlos Lorca Tobar 964, Independencia, 81380494, Santiago, Chile. E-mail: proberts@uchile.cl. Telephone number: +56229781666.

Abstract

Encapsulation of quercetin (Q) with inulin (In) by spray-drying was performed applying a Box-Behnken design where the effect of the inlet air temperature, percentage of inulin crystallite dispersion and Q content were studied on the crystallinity index (CI). Three microparticle systems with CI between 2% and 20% (Q-In-2%, Q-In-12% and Q-In-20%) were selected to study the CI effect on Q release during an *in vitro* digestion. The higher the CI of microparticles, the higher the encapsulation efficiency (76.4%, Q-In-20%). Surface quercetin was steadily released during the oral, gastric, and intestinal phases of the digestion. The CI of the microparticles did not influence the Q bioaccessibility values (23.1 to 29.7%). The highest Q delivery occurred during the simulated colonic phase (44.4 to 66.4%) due to the action of the inulinase. The controlled crystallization in spray-dried microparticles is a promising strategy for the designing of polyphenol-based microparticles with specific delivery properties.

Keywords: microencapsulation, spray drying, crystallinity, flavonoid, encapsulating agent, digestion.

Abbreviations

Q: Quercetin; In: Inulin; CI: Crystallinity index; EE: Encapsulation efficiency; DP: Degree of polymerization; RSM: Response surface methodology, ANOVA: Analysis of variance; SEM: Scanning electron microscopy; AFM: Atomic force microscopy; MDSC: Modulated differential scanning calorimetry; T_g: Glass transition temperature; T_c: Crystallization temperature; T_m: Melting temperature; T_d: Degradation temperature; H_c: Crystallization enthalpy; H_m: Melting enthalpy; H_d: Degradation enthalpy.

1. Introduction

Currently, the food industry has a great interest in the development of polyphenol-based foods due to their healthy claims. Quercetin is one of the most common flavonoids found in vegetables and fruits. Among the beneficial effects on health, such as antioxidant, anticancer or antiviral properties, quercetin has been also reported to prevent and attenuate chronic inflammatory disorders (Jantan et al., 2021). However, the oral administration of quercetin using foods as delivery vehicles is challenging due to its poor water solubility (Srinivas et al., 2010). In this context, encapsulation technologies have been reported to enhance the stability of the bioactive encapsulated against environmental, food processing, or digestive conditions, improving their solubility and bioavailability after ingestion, masking unpleasant taste and flavor and promoting controlled release (Estevinho & Rocha, 2018; Maqsoudlou, Mohebodini & Jafari, 2020).

Spray drying is one of the most widely used to encapsulate bioactive compounds (Maqsoudlou et al., 2020). Spray-dried microparticles can be designed to optimize the release of bioactive encapsulated either with a techno-functional purpose or along the gastrointestinal tract. When the goal is the controlled release under digestive conditions, some properties of the encapsulating agent have been considered, such as solubility (Desai, Stanley, & Murthy, 2020; Gavini et al., 2005), degradation or erosion by digestive enzymes (Davidov-Pardo, Arozarena, & Marín-Arroyo, 2013), the response to pH changes (González et al., 2019; Moreno, Cocero, & Rodríguez-Rojo, 2018), or the mixture of several polymers mixtures (Ahmadian, Niazmand, & Pourfarzad, 2019; Ruiz Canizales et al., 2019).

Another strategy to design microparticles with specific characteristics of release of the encapsulated bioactive compounds is to modify some of their physicochemical properties (Boostani & Jafari, 2021). Crystallinity is an important physical property of spray-dried powder since it can affect both the flowability of the powder and its stability during storage (Ronkart et al., 2009a). Although in general, amorphous powders are resultant from the spray-drying process due to the fast water evaporation during the atomization (Ronkart et al., 2007), the modification of the crystallinity index (CI) could be a strategy to control the release of bioactive compounds from spray-dried microparticles in the gastrointestinal tract. To the best of our knowledge, the effect of the degree of crystallinity of the microparticles on the bioactive release during gastrointestinal digestion has only been addressed in a few

81 studies, such as Ahmadian et al. (2019), where blends of maltodextrin-pectin were used to
82 encapsulate saffron petal phenolic extract.
83 Among the encapsulating agents, inulin is an interesting biopolymer due to its health benefits
84 and colonic release properties (Mensink et al., 2015). Inulin is a non-digestible
85 polysaccharide, composed of fructose chains linked by β-(2-1)-D-fructosyl-fructose bonds
86 and one terminal α-D-(1-2)-glucose (Ronkart et al., 2007). Inulin spray-dried powders can
87 have different amorphous/crystalline physical states. Spray-drying processing variables, such
88 as the infeed temperature and the inlet air temperature, have been described as modulators of
89 the CI of spray-dried inulin powders (Ronkart et al., 2007; Ronkart et al., 2009a).
90 In addition, the amorphous/crystalline physical state found in inulin powders is dependent on
91 the crystallinity properties of the infeed suspension. Ronkart et al. (2007) obtained
92 amorphous and semicrystalline inulin powders from transparent and milky or cloudy inulin
93 suspensions, respectively. Crystalline states of inulin have been produced by cooling aqueous
94 concentrated solutions at 20% w/v (Glibowski & Pikus, 2011; Romano et al., 2018), 21%
95 w/v (Morelo et al., 2019) and between 30% to 45% w/v (Hébette et al., 1998); or by
96 suspending 20% w/v of inulin in water at temperatures in the range 40-80 °C (Ronkart et al.,
97 2007; Ronkart et al., 2009a). Besides concentration, the polymerization degree, the heating
98 and cooling temperature and rate, the pH, the solvent used in solubilization, the presence of
99 crystals to initialize the crystallization, and the crystallization time have been shown to
100 influence the formation of inulin crystals in the solution (Glibowski & Pikus, 2011; Hébette
101 et al., 1998, Kim, Faqih, & Wang, 2001). Therefore, this study states as a hypothesis that the
102 mixture of inulin dispersions with inulin crystallite dispersions at different ratios may control
103 the final crystallinity of the resulting inulin powders. To the best of our knowledge, this
104 strategy has not been studied yet to encapsulate polyphenols by spray-drying.
105 Nowadays, inulin with different CI has been used as encapsulating agent in
106 microencapsulation by spray-drying only in two studies, and none of them have evaluated
107 the performance of the obtained microparticles as delivery systems of bioactive compounds
108 during gastrointestinal digestion. Morelo et al. (2019) studied the effect of amorphous and
109 semicrystalline inulin microparticles with quercetin or epicatechin on the oxidative stability
110 of lipidic matrices. On the other hand, Romano et al. (2018) evaluated the stability of *L.*

plantarum during the spray-drying encapsulation process and on storage conditions using amorphous and semicrystalline inulin as encapsulating agents.

The objective of this study was to design spray-dried quercetin microparticles with different crystallinity indexes using mixtures of inulin and inulin crystallite dispersions as encapsulating agent, and to evaluate the influence of the crystallinity index on the physicochemical, thermal, and morphology properties of the microparticles, as well as on the release profile of quercetin under *in vitro* simulated gastrointestinal digestion.

2. Materials and Methods

Quercetin (Q, purity ≥ 95%) was obtained from Sigma-Aldrich (Santiago, Chile). Inulin Orafti® HP (degree of polymerization, DP ≥ 23) was obtained from Blumos S.A. (Santiago, Chile). Pepsin from porcine gastric mucosa (P7012, 2500 AU/mg), pancreatin from porcine pancreas (P7545, 8 x USP specifications), bile extract (B8631), and inulinase (*Aspergillus niger*, 23.6 U/mg) were purchased from Sigma-Aldrich (Santiago, Chile).

2.1 Formulation of quercetin-inulin microparticles

Two inulin dispersions were prepared as follows:

Inulin dispersion: Inulin (12.6% w/w) was dispersed in distilled water under stirring for 15 min at 25 °C.

Inulin crystallite dispersion: Inulin (12.6% w/w) was dispersed in distilled water and heated at 70 ºC under stirring. Afterward, the dispersion was cooled up to 20 °C at a cooling rate of 1.2 °C/min, using a double-layer jacketed glass beaker connected to a recirculating bath (JSRC-13C, JS Research, Korea). The dispersion was kept under stirring for 48 h at 140 rpm and 10 ºC in an orbital shaker (JSSI-100C, JS Research, Korea).

Both inulin dispersions were mixed at different ratios to obtain spray-dried powders with different CI, according to the following experimental design (Table 1).

The encapsulation of quercetin with inulin was performed by spray drying, applying a Box Behnken design (15 runs, 12 experimental points, and 3 central points). The independent variables were the inlet air temperature (120 to 200 ºC), percentage of inulin crystallite dispersion (0 to 100%), and quercetin content (0.2 to 0.5 g); whereas the response variable was the CI.

Quercetin-inulin infeed dispersion was prepared as follows: the inulin dispersion and the inulin crystallite dispersion were mixed according to the statistical design, then quercetin (0.2 to 0.5 g) in ethanol (10 g) was added to the mixture, stirring for 30 min at 20 ºC. Infeed dispersions were fed into a mini spray-drying (B-290, Büchi, Switzerland). The process conditions were: airflow of 600 L/h, atomization pressure of 20 psi, rate of feeding of 2 mL/min, infeed temperature of 20 ºC, and inlet air temperature between 120 °C and 200 ºC (according to the experimental design). The powders obtained were stored inside Falcon tubes in a vacuum desiccator with silica gel and protected from light.

The response surface methodology (RSM) was applied to each independent variable and the response variable (CI) was maximized. Analysis of variance (ANOVA), lack of fit, and determination of the regression coefficients were performed using the software Statgraphics (7.0 program, Manugistics Inc., Rockville, MA). Data were fit to a second-order regression model (Eq. 1), considering linear, quadratic, and cross-product forms of the inlet air temperature, percentage of inulin crystallite dispersion, and quercetin content.

$$Y = \beta_0 + \beta_1 X_1 + \beta_2 X_2 + \beta_3 X_3 + \beta_{12} X_1 X_2 + \beta_{13} X_1 X_3 + \beta_{23} X_2 X_3 + \beta_{11} X_1^2 + \beta_{22} X_2^2 + \beta_{33} X_3^2 + \varepsilon \quad \text{(Eq. 1)}$$

Where Y was the estimated response; X_1, X_2, X_3 are the levels of the independent variables; β_0 was the intercept term; β_1, β_2 y β_3 the linear coefficients; β_{12}, β_{13} y β_{23} the interaction coefficients; β_{11}, β_{22} y β_{33} the quadratic coefficients and ε the error.

According to the results of the experimental design, three microparticle systems with the lowest (2%), the highest (20%) and an intermediate (12%) CI values (Q-In-2%, Q-In-12% and Q-In-20%) were selected.

2.2 Characterization of the quercetin microparticles

The three microparticle systems selected (Q-In-2%, Q-In-12%, and Q-In-20%) were characterized according to the following parameters.

2.2.1 Crystallinity index

X-ray scattering patterns were determined with a SAXSPoint 2.0 system (Anton Paar, Austria). This instrument was equipped with a microfocus copper X-Ray source (Primus 100, Cu Kα = 1.54178 Å) operated at 50 kV and 100 μA, an ASTIX multilayer mirror for point collimation and an Eiger R 1M bidimensional detector (Dectris, Baden-Daettwil, Switzerland). Microparticles were confined into a 1.0 mm diameter thin-walled special glass capillary tube (Charles Supper Company, USA). One frame of 900 s exposure time was recorded at 25 °C using a sample detector distance of 115 mm. The obtained patterns were reduced with SAXSDrive software (Anton Paar), accounting for sample transmission and capillary tube scattering subtraction before being integrated into 1D scattering intensities as a function of the magnitude of the scattering vector q ($q = (4\pi/\lambda)\sin\theta$; where 2θ is the total scattering angle).

The CI was determined between 5 and 35º in 2θ. A smooth amorphous curve was drawn over the base of the crystalline peak following the pattern of an inulin amorphous sample. Then, the amorphous curve was subtracted, and the area of the peaks (crystalline fraction) was integrated (Mali et al., 2006). The ratio of the area of the crystalline peaks to the total area was considered as the CI of the sample by application of equation 2.

$$CI\ (\%) = \frac{Integrated\ intensity\ of\ crystal\ peaks}{Total\ integrated\ intensity\ of\ scattering} \cdot 100 \qquad \text{(Eq. 2)}$$

2.2.2 Encapsulation efficiency

Total quercetin: Q-In-2%, Q-In-12% and Q-In-20% microparticles (100 mg) were dispersed in 3 mL of milli-Q water at 75 ºC. The mixture was stirred using a vortex mixer for 1 min and sonicated for 5 min, twice. The same procedure was performed by adding methanol (3 mL). The mixture was centrifuged for 10 min at 10050 *g* (Hettich Universal 320R, Germany) and 4 ºC. The supernatant was removed and transferred to a volumetric flask (25 mL). The pellet was redispersed in milli-Q water:methanol (20:80 v/v), applying the same procedure described above (vortex, sonication, and centrifugation). The supernatant was also transferred to a volumetric flask and filled up with methanol. Then an aliquot (5 mL) was filled up to 10 mL with methanol and injected into the HPLC.

Surface quercetin: Q-In-2%, Q-In-12% and Q-In-20% microparticles (100 mg) were dispersed in 4 mL of methanol:water (50:50 v/v) by gentle stirring. An aliquot of 2 mL was centrifuged at 3100 *g* for 3 min. The supernatant was removed and transferred to a volumetric flask (10 mL), filled up with methanol, and then injected into the HPLC.

Chromatographic analysis: Quercetin determination was performed by HPLC, using an Alliance e2695 (Waters, USA) chromatograph equipped with a photodiode-array detector (Waters 2998, Waters, USA) and a C18 column (5 µm, 4.6 mm i.d. x 250 mm, Symmetry, Waters, Dublin, Ireland). The isocratic mobile phase was milli-Q water:methanol:acetonitrile (45:40:15 v/v/v) containing 1% glacial acetic acid at a flow rate of 1 mL/min (Palma et al., 2014). Quercetin was quantified using a calibration curve (1-100 µg/mL; $R^2 = 0.99$).

2.2.3 Recovery

The quercetin recovery was determined according to equation 3:

$$Recovery\ (\%) = \frac{Total\ quercetin\ in\ the\ microparticles}{Theoretical\ total\ quercetin\ in\ the\ microparticles} \cdot 100 \qquad \text{(Eq. 3)}$$

2.2.4 Solubility

Solubility was determined according to Cano-Chauca et al. (2005). Briefly, Q-In-2%, Q-In-12%, and Q-In-20% microparticles (100 mg) were dispersed in distilled water (10 mL), stirred for 5 min, and centrifuged at 1110 *g* for 5 min. An aliquot (2.5 mL) was dried at 105 °C in an oven (BE 500, Memmert ®, Schwabach, Germany) for 5 h. The dry weight of the soluble solid was registered, and solubility was expressed as a percentage.

2.2.5 Moisture content, hygroscopicity, and water activity

The moisture content of the microparticles (between 0.5 and 0.7 g) was determined using an infrared moisture analyzer (PMR50/NH, Radwag Miami, FL, USA). The water activity of microparticles (1 g) was measured by the determination of the dew point (Hygrolab2, Rotronic, Hauppauge, NY, USA) at 20 ± 3 ºC. The hygroscopicity was measured gravimetrically according to Cai & Corke (2000). Microparticles (1.5 g) in a clock glass were placed in a desiccator with Na_2SO_4 (81% relative humidity) for one weak at 25 ºC.

232

233 *2.2.6 Thermal analysis*

234 The thermal behavior was evaluated by modulated differential scanning calorimetry (MDSC;
235 TA Q20, TA Instruments, USA). Microparticles (between 5 and 7 mg) were placed in sealed
236 aluminum pans (TZero®, internal volume of 10 μL). Thermograms were obtained over a
237 temperature range from 10 to 250 °C with a heat rate of 1.5 °C/min. The amplitude and period
238 of the modulated heat flow were 1.5 °C and 90 s, respectively. The Universal Analysis 2000
239 software (v4.5A, TA Instruments New Castle, DE, USA) was used to determine the thermal
240 transitions. The glass transition temperature was determined from the reverse heat flow
241 curves, while the recrystallization, melting, and degradation temperatures and enthalpies
242 were determined from the heat flow curves.

243

244 *2.2.7 Particle size*

245 Particle size and particle size distribution were analyzed by light scattering using a laser
246 scattering particle size analyzer (Partica LA-960, Horiba, Japan; 650 nm laser diode).
247 Microparticles were dispersed in ethanol and the particle size was expressed as volume mean
248 diameter ($D_{4,3}$).

249

250 *2.2.8 Morphology of the microparticles*

251 The morphology and external structure of the microparticles (Q-In-2%, Q-In-12%, and Q-
252 In-20%) were analyzed by scanning electron microscopy (SEM) and atomic force
253 microscopy (AFM).

254 The SEM images were obtained with a High-Resolution Scanning Electron Microscopy (FE-
255 SEM, Inspect-F50, FEI, Netherlands) using a secondary electron detector operated at 2 kV.
256 Microparticles were covered with a 10 nm gold film using a Sputter Coater (Cressington
257 model 108, Ted Pella Inc., USA) equipped with a thickness controller (Cressington MTM-
258 20). Images were obtained using the software EDS 7424 (Oxford Instruments, Oxford, UK).
259 The AFM images were obtained with an Anton Paar Tosca 400 microscope (Anton Paar,
260 Graz, Austria), in tapping mode with Arrow™ NCR cantilever (NanoWorld® AG,
261 Neuchâtel, Switzerland). The cantilever was automatically calibrated at 221.12 kHz resonant
262 frequency. The images were captured at three magnifications, rastering 25x25 μm, 5x5 μm,

and 1.5x1.5 µm at a scanning speed of 0.2 lines per second with 500 points per line resolution. The samples were immobilized in epoxy resin. Microparticles were powdered on the resin and the excess was blown away with nitrogen. The samples were left to fully cure overnight before being measured.

2.3 *In vitro* simulated gastrointestinal digestion

The performance of the three microparticle systems selected (Q-In-2%, Q-In-12%, and Q-In-20%) as quercetin delivery systems was evaluated under simulated gastrointestinal digestion. The digestion phases (oral, gastric, and intestinal) were simulated according to the INFOGEST 2.0 protocol (Brodkorb et al., 2019) with some modifications. The microparticles (1.3 g, containing 42 mg de quercetin) were dispersed in distilled water (5.2 mL). Afterward, the simulated salivary fluid (5.2 mL), 0.3 M $CaCl_2$ (32.5 µL), and distilled water (1.268 mL) were added, and the oral dispersion was incubated at 37 °C for 2 min at 250 rpm in a magnetic stirrer with a temperature controller (Heidolph Instruments, Germany). At the end of the oral digestion, an aliquot of 0.5 mL was taken and stored at -20 ºC. Afterward, the simulated gastric fluid (10 mL) and 0.3 M $CaCl_2$ (6.3 µL) were added to the oral digestion. The pH was adjusted to 2 with 1M HCl and pepsin (2000 U/mL gastric phase) was incorporated. The dispersion was incubated at 37 ºC for 2 h and 250 rpm. During the gastric digestion, aliquots of 0.3 mL were withdrawn at intervals of 30 min and stored at -20 ºC. Finally, the simulated intestinal fluid (10.12 mL) and 0.3 M $CaCl_2$ (48 µL) were incorporated, and the pH was adjusted to 7 with 1M NaOH. Afterwards, the bile extract and pancreatin (trypsin activity of 100 U/mL intestinal phase) were added, and the dispersion was incubated at 37 ºC for 2 h and 250 rpm. During the intestinal digestion, aliquots of 0.3 mL were withdrawn every 30 min and stored at -20 ºC. After the intestinal phase, samples were centrifuged at 380 *g* for 10 min at 4 ºC. The pellet was dispersed in phosphate buffer (0.05 M, pH 6.8) and inulinase (5 U/mL) was added to simulate the colonic phase of digestion (Jain et al., 2014). The dispersion was incubated at 140 rpm for 24 h and 37 °C in an orbital shaker (JSSI-100C, JS Research, Korea). Aliquots (500 µL) were collected at 18 and 24 h and stored at -20 ºC.

Digestion of microparticles without surface quercetin: Q-In-20% microparticles were subjected to surface quercetin removal. The microparticles (500 mg) were dispersed in

methanol (20 mL), softly stirred, and filtered through a filter paper (Whatman N°1). The filter paper was subjected to 30 °C for 20 min inside an incubator (JSSI-100C, JS Research, Korea). The process was repeated four times to have enough amount of sample. Dry powder was collected and subjected to simulated gastrointestinal digestion according to the INFOGEST 2.0 protocol, as previously detailed.

2.3.1 Determination of quercetin released

Quercetin released from the microparticles (Q-In-2%, Q-In-12%, and Q-In-20%) at specific times of each digestion phase (oral, gastric, and intestinal) was determined as follows: the aliquots collected after every digestion phase were thawed and centrifuged for 10 min at 380 *g* and 4 °C. An aliquot (150 µL) of the supernatant was added to methanol (1350 µL), vortexed for 1 min, and centrifuged at 2430 *g* for 10 min and 4 ºC. The supernatant was filtered (0.22 µm Millipore filter) and injected into the HPLC following the procedure described in 2.2.2. In the colonic phase, Q was extracted by adding 1.5 mL of methanol. The mix was vortexed for 30 s and centrifuged at 2430 *g* for 10 min and 4 °C. The supernatant was filtered (0.2 µm Millipore filter), diluted twice, and centrifuged at 9720 *g* for 10 min and 4 °C. Quercetin was measured by HPLC according to section 2.2.2.

2.3.2 Optical microscopy

Photomicrographs were taken during the *in vitro* simulated digestion. Drops of the digested samples were withdrawn at the end of the oral phase, as well as at the beginning and the end of the gastric and intestinal phases. The drop was placed onto a cover glass and covered with another one. A polarized light microscope (DLMP, Leica, Germany), coupled with a Canon EOS 750D camera, was used to obtain the photomicrographs with 100X magnification.

2.4 Statistical analysis

All the determinations were performed in triplicate. One-way ANOVA and Tukey´s multiple range test were applied to determine the statistical differences among samples, using the Statgraphics software (version 7.0, Manugistics Inc., Statistical Graphics Corporation, USA).

3. Results and discussion

3.1 Formulation of quercetin-inulin microparticles

A Box-Behnken experimental design was applied to study the effect of the percentage of inulin crystallite dispersion, quercetin content, and inlet air temperature on the CI of the microparticles.

Table 1 shows the experimental design and analysis of variance (ANOVA) for encapsulation of Q with inulin by spray-drying. The CI of the microparticles ranged between 2.1% and 20.1%. The linear forms of the inlet air temperature and the percentage of inulin crystallite dispersion, as well as the cross-product form between both variables, were significant ($p \leq 0.05$) on the CI of the microparticles. The model explained 89.1% of the variability (R^2 adjusted for degrees of freedom) in CI.

The surface graphic (Figure 1 a-c) shows that the CI of the microparticles increased with increasing the percentage of inulin crystallite dispersion in the infeed, especially at low temperatures (120 to 160 °C) (Figure 1a). Moreover, the higher the inlet air temperature the lower the CI of the microparticles, since high temperatures may induce the melting of the preformed inulin crystals in the infeed. Similarly, Ronkart et al. (2009a) found a partial melting of the inulin crystals contained in the infeed during the spray drying process.

The percentage of inulin crystallite dispersion (100%) and quercetin content (0.5 g) to maximize CI were in the upper limit of the range studied, whereas inlet air temperature (120 ºC) was in the lower limit of the range studied. According to the results of the experimental design, three microparticle systems with the lowest (2%), the highest (20%) and an intermediate (12%) CI values (Q-In-2%, Q-In-12% and Q-In-20%) were selected to study the CI effect on Q release during an *in vitro* digestion. Table 2 shows the experimental percentages of inulin crystallite dispersion in the infeed (formulation variable) and inlet air temperatures (process variable) to obtain Q-In-2%, Q-In-12% and Q-In-20% microparticles: 0% inulin crystallite dispersion/200 ºC (Q-In-2%), 50% inulin crystallite dispersion/160 ºC (Q-In-12%), and 100% inulin crystallite dispersion/120 ºC (Q-In-20%). The quercetin content was 0.35 g/100 g infeed in all the microparticle systems.

3.2 Characterization of quercetin inulin microparticles

Table 2 shows the characterization of Q-In-2%, Q-In-12% and Q-In-20% microparticles.

3.2.1 Crystallinity index

The CI values increased with the increase of the percentage of inulin crystallite dispersion in the infeed and the decrease of the inlet air temperature (Table 2). The highest CI values were obtained with the highest percentage of inulin crystallite dispersion (100%) and the lowest inlet air temperature (120 ºC), since a low inlet air temperature prevents the melting of the inulin crystallites during the spray-drying. Higher CI values were reported by Morelo et al. (2019) and Ahmadian et al. (2019) for quercetin microparticles with inulin (60%) and saffron petal phenolic extract microparticles with maltodextrin and pectin (45% and 60%), respectively. In fingered citron extract microparticles with blends of maltodextrin, gum arabic, modified starch, and whey protein, the CI ranged between 18.2% and 46.1% (Mahdi et al., 2020). Thus, structural features of the biopolymers and both formulation (infeed dispersion or crystal dispersion) and operational spray drying conditions may influence the crystallinity of the microparticles.

The X-ray diffractograms patterns for Q-In microparticles and empty inulin microparticles (In) at three crystallinity indexes (2%, 12%, and 20%), are shown in Figure 2 (a and b, respectively). Both Q-In-2% and In-2% systems showed a broad halo pattern typical of an amorphous state. However, tiny peaks at 12.9º and 27.0º in 2θ (Figure 2a) were found in Q-In-2% microparticles, attributed to crystalline quercetin domains (supplementary material, Figure S1). Similar results were reported by Morelo et al. (2019) in semicrystalline quercetin-inulin microparticles.

Q-In microparticles with CI 12% and CI 20% showed characteristic diffraction peaks of a semicrystalline state. Hemihydrate and monohydrate forms have been reported for semicrystalline inulin (André et al., 1996). The structure of these two forms only changes in the amount of water in the unit cell, yielding similar diffraction patterns that mainly differ in the presence of a sharp peak at 10.6°, characteristic of the hemihydrate inulin form. In the semicrystalline Q-In microparticles (Figure 2a) and empty In microparticles (Figure 2b) with CI 12% and 20%, the absence of the peak at 10.6° indicated the existence of orthorhombic monohydrated inulin polymorph in these microparticle systems (André et al., 1996).

3.2.2 Encapsulation efficiency and recovery of quercetin

Encapsulation efficiency (EE) is an important parameter to evaluate the encapsulation process by spray-drying, and it represents the quercetin-inulin interaction by hydrogen

bonding, electrostatic interactions, hydrophobic interactions, or Van der Waals forces. The EE of quercetin ranged from 70.5% to 76.4% (Table 2). The EE of quercetin increased ($p \leq 0.05$) with increasing the CI of the microparticles (Table 2), which may be attributed to the orthorhombic unit cell arranged by crystalline inulin, leaving the hydroxyl groups more exposed to interact with quercetin and therefore increasing the EE. The same trend in EE of quercetin, but with lower EE values, was reported by Morelo et al. (2019) for amorphous and semicrystalline quercetin-inulin microparticles (51.1% and 67.8%, respectively). Other studies have reported EE values of 18.5% (Sun-Waterhouse, Wadhwa, & Waterhouse, 2013) and 73.3% (Ayala-Fuentes et al., 2022) for quercetin in inulin microparticles, but the CI was not determined.

Studies dealing with the encapsulation of polyphenols with crystalline biopolymers by spray-drying are scarce. According to Ahmadian et al. (2019), the EE of polyphenols ranged from 68.2% to 86.7% in saffron petal phenolic extract microparticles with maltodextrin and different pectin contents, and the EE values increased with an increase in the pectin content since pectin provided crystallinity to the microparticles. In another study, where fingered citron extract was encapsulated with gum arabic, maltodextrin, modified starch, and whey protein, the CI ranged from 18.2% to 46.1%. However, the EE was not related to the CI (Mahdi et al., 2020).

Polyphenols may be degraded during the spray-drying process, and the recovery represents the loss of polyphenols that may occur. The recovery of quercetin reached values above 90% for Q-In (IC 2%, 12%, and 20%, Table 2), showing that quercetin was stable despite the high drying temperatures. Morelo et al. (2019) reported lower recovery values (75% to 78%) for quercetin encapsulated with inulin.

3.2.3 Moisture, water activity, hygroscopicity, and solubility

The moisture of the microparticle systems ranged from 2.29% to 2.84% (Table 2). Q-In-20% had the highest moisture, attributed to the lowest inlet air temperature applied during spray-drying (120 °C). Therefore, the moisture content in the Q-In microparticles was inversely proportional to the inlet air temperature (Cai & Corke, 2000).

The water activity of Q-In microparticles ranged from 0.206 to 0.256 (Table 2). Although amorphous microparticles (Q-In-2%) had significantly higher water activity than

semicrystalline microparticles (Q-In-12% and Q-In-20%), all the microparticle systems showed water activity values low enough to ensure the microbiological stability of the powders (Karrar et al., 2021).

Hygroscopicity ranged from 17.6 to 29.5 g/100 g (Table 2) for Q-In microparticles. Although amorphous microparticles have been reported to be more hygroscopic than semicrystalline ones (Karrar et al., 2021; Mahdi et al., 2020), the microparticles with the lowest CI (Q-In-2%) showed the lowest hygroscopicity in this study. This behavior may due to the crystallization of the amorphous regions of these microparticles during the hygroscopicity determination (7 days at 81% RH), and the formed crystals may lead to the release of water from the matrix or may act as crosslinking agents that restrict the mobility of chains. Therefore, the structural features of the inulin and its physical state (amorphous/crystalline) determine the hygroscopicity of the microparticles.

The solubility of the microparticles decreased as the crystallinity increased. The microparticles with the highest CI (Q-In-20%) showed the lowest solubility values. The crystallinity of the microparticles influences their rehydration properties since crystalline powders are less wettable in water and dissolve more slowly than amorphous powders (Botrel et al. 2016).

3.2.4 Particle size

The particle size ($D_{4,3}$) of the Q-In microparticles (Table 2) was not significantly affected ($p \geq 0.05$) by the CI. However, the particle size showed a tendency to decrease with increasing crystallinity, as reported by Morelo et al. (2019). The particle size distribution was unimodal in all the microparticle systems (supplementary material, Figure S2). The width of the particle size distribution (determined according to Goëlo et al., 2020) showed values close to 0.7, 0.6 and 0.5 μm for Q-In-2%, Q-In-12% and Q-In-20%, respectively. Thus, amorphous microparticles had a wider particle size distribution, which may be related to their greater tendency to agglomeration.

3.2.5 Morphology of the microparticles

SEM images of Q-In microparticles (Q-In-2%, Q-In-12% and Q-In-20%) are shown in Figure 2 (c-e, respectively). The differences found in morphology among the microparticle systems

may be explained by the crystallinity of the microparticles. The amorphous microparticles (Figure 2c, Q-In-2%) had spherical shape and smooth surface, some of them with slight indentations on their surface. In contrast, the most semicrystalline microparticles (Q-In-20%, Figure 2e) showed irregular spiral shapes and rough surfaces, suggesting that this morphology would be attributed to inulin conformation. In fact, inulin chains have been reported to adopt a helical conformation with lamellar arrangements of antiparallel chains (André et al., 1996, Barclay et al., 2016). However, the irregular spiral shape has not been previously reported for inulin with different CI by spray-drying (Morelo et al., 2019; Romano et al., 2018; Ronkart et al., 2007). The morphology may be influenced by formulation and process variables, such as inulin concentration in the infeed and crystallization time, among others. Q-In-12% showed spherical and irregular spiral shapes (Figure 2d), in line with its intermediate CI. Ronkart et al. (2007) also found morphological differences between amorphous and semicrystalline inulin microparticles, related to the properties of the infeed solution. In that study, microparticles with a smooth or rough surface were obtained when inulin infeed was a solution or a suspension (undissolved solid particles). Therefore, the two kinds of microparticle populations in Q-In-12% may be due to the mixture of inulin and inulin crystallite dispersions in the infeed.

The particle size and morphology for Q-In-2% and Q-In-20% were also evaluated by AFM (Figure 2 f-h). The size of the microparticles were in accordance with the $D_{4,3}$ values in Table 2. Q-In-2% and Q-In-20% showed a different topology, as can observed in the AFM images (supplementary material, Figure S3). Amorphous microparticles (Q-In-2%) primarily showed a homogeneous surface with the inclusion of segregated material in microdomains, which may be attributed to quercetin. In the case of the semicrystalline microparticles (Q-In-20%), a locally heterogeneous composition of the surface was found throughout the whole particle. This suggests a more homogeneous inclusion of quercetin in the semicrystalline microparticles than in the amorphous ones. The AFM is a useful technique that provides qualitative (morphology) and quantitative (roughness) data on the surface morphology of various materials (Herrmann et al., 2004).

3.2.6 Thermal properties

Table 3 shows the thermal properties of the Q-In and In microparticles with three different CI (2%, 12%, and 20%). As the temperature increases in the thermal profile (supplementary material, Figure S4), several events can be found: (1) a glass transition (T_g), (2) a cold recrystallization event (T_c, ΔH_c) due to the rearrangement of the amorphous fraction, (3) one or more melting events (T_m, ΔH_m) attributed to the melting of different crystal populations, and (4) an endothermic peak associated with the inulin degradation (T_d, ΔH_d).

In both Q-In and In microparticle systems, the T_g decreased as the CI of the microparticles increased due to the crystallinity promotes a change in the molecular weight distribution of the amorphous fraction of the microparticles. During the preparation of the semicrystalline microparticles infeed (Q-In-12%, Q-In-20%, In-12%, and In-20%), the higher molecular weight fractions will start to precipitate/crystallize. The remaining inulin in the solution will be enriched in low molecular weight fractions that yield the amorphous fraction of the microparticles, which is responsible for T_g values. The amorphous fraction with a higher proportion of low-molecular-weight inulin requires lower energy to increase their mobility and give lower T_g values. This fractionated crystallization has been reported for inulin by Hébette et al. (1998). Moreover, the higher water content found in Q-In-20% may contribute to the lower T_g values in this microparticle system, since water is known to act as a plasticizer, decreasing T_g values (Ronkart et al., 2009b). Therefore, the storage temperature of the microparticles must be below the T_g (in a glassy state), decreasing both molecular mobility and quercetin degradation.

Regarding cold crystallization, both T_c and ΔH_c decreased as the CI of the microparticles increased, both in Q-In and In microparticles systems, which may be also attributed to the modification of the molecular weight distribution of the amorphous fraction of the microparticles. Furthermore, the lower T_c found in Q-In-20% may also be associated with its higher water content, which acts as a plasticizer, in accordance with Ronkart et al. (2009b).

Q-In-2% only showed one melting event (168.9 ºC), whereas two melting events were found in Q-In-12%, at around 161.1 ºC and 168.7 ºC, and three melting events were found in Q-In-20% (136.3 ºC, 146.2 ºC, and 163.7 ºC). The differences in the number of inulin melting events have been attributed to different crystal populations with different shapes, perfection, size, and molecular weight distribution (Romano et al., 2018; Ronkart et al., 2007; Ronkart et al., 2009a). The endothermic peak found at the highest temperature (T_{m3}) corresponded

mainly to the melting of the crystals formed during the cold crystallization of the amorphous fraction for Q-In-2%. While for Q-In-12% and Q-In-20%, T_{m3} represented mainly the melting of crystals fraction present in microparticles. Melting events for Q-In-12% (T_{m2} and T_{m3}) and Q-In-20% (T_{m1}, $T_{m2,}$ and T_{m3}) corresponded to inulin crystals present in the infeed (section 2.1.), which were responsible for the peaks found in the X-ray diffractogram, as well as from cold crystallization. Q-In-20% showed a shift of the T_{m3} towards significantly lower temperatures (163.7 ºC) than Q-In (CI 12% and 2%), which may be attributed to the fractionated segregation of molecular weight distributions in Tm_1 and Tm_2, and for its higher water content that acts as a plasticizer, as described by Ronkart et al. (2009b).

3.2.7 In vitro simulated digestion

Figure 3 shows the release profile of quercetin from Q-In-2%, Q-In-12% and Q-In-20% microparticle systems during the oral, gastric and intestinal phases of the simulated digestion. The release of quercetin in the oral phase ranged from 3.6 to 10.3%, and it was significantly higher for the system with the highest CI (Q-In-20%; 10.3 ± 1.2%). The quercetin released in the gastric phase reached values between 3.5% and 10.3%, where the amorphous system (Q-In-2%) showed the highest release of quercetin at the end of the gastric digestion (10.3 ± 2.2%), whereas the quercetin released from Q-In-12% and Q-In-20% underwent some degradation (~6%). The quercetin released during the intestinal phase increased for the three Q-In microparticle systems studied (23.1 to 29.7%), which may be attributed to the incorporation of quercetin to the micelles formed from the bile salts during this digestion phase. There were no significant differences between Q-In-20% and Q-In-2% in the release of Q at the end of the intestinal phase. Considering that the EE of Q-In-2%, Q-In-12% and Q-In-20% was 70.4%, 72.1% and 76.4%, the surface quercetin was 29.6%, 27.9% and 23.6%, respectively. Therefore, the quercetin released from Q-In-2% (27.4%; Figure 3) and Q-In-12% (23.1%; Figure 3) corresponded to the surface quercetin, whereas the quercetin released from Q-In-20% (29.7%; Figure 3) corresponded to the surface quercetin plus some of the quercetin encapsulated into the microparticles (~6%). To verify this assumption, washed microparticles of Q-In-20% (without surface quercetin) were subjected to *in vitro* simulated digestion (Figure 3, continuous line). This profile showed that some of the encapsulated quercetin (~7.4%) was released in the intestinal phase, similar to unwashed microparticles

(~6%). Ahmadian et al. (2019) reported a sustained release of encapsulated saffron petal phenolic extract from spray-dried maltodextrin-pectin microparticles in the simulated digestion. The increase in pectin percentage in the microparticles increased both the crystallinity of the microparticles and the phenolic compounds released during the digestion (Ahmadian et al., 2019). The release of the phenolic compounds was higher than in this study because the biopolymers used as encapsulating agents were water soluble and susceptible to hydrolysis by intestinal enzymes.

The bioaccessibility of quercetin was 27.4 ± 1.0%, 23.1 ± 1.0% and 29.7 ± 1.2% for Q-In-2%, Q-In-12% and Q-In-20%, respectively, at the end of the intestinal digestion. Thus, the bioaccessibility of quercetin was very close in the three microparticle systems because the CI did not affect the release of quercetin, where surface quercetin was mainly released in the intestinal phase. Inulin has been reported as a colon-specific delivery biopolymer because the human upper gastrointestinal tract lacks enzymes to cleave β-(2-1) linkages in the fructose (Mensink et al., 2015), which together with the low water solubility of quercetin (2.15 μg/mL; Srinivas et al., 2010), may explain the low release of quercetin from the microparticles during the simulated digestion and the low bioaccessibility values.

The *in vitro* simulated gastrointestinal digestion for Q-In-2% and Q-In-20% microparticles was followed through photomicrographs (Figure 3). Differences in dispersibility were noticed depending on the amorphous/semicrystalline physical state of the microparticles. In the oral phase, Q-In-2% microparticles formed small clumps, while Q-In-20% were more dispersible and clumps were not found. Glibowski & Pikus (2011) reported a similar behavior in the dispersibility of semicrystalline and amorphous inulin powder in contact with water. The presence of clumps and the characteristic dispersibility of each microparticle system is maintained during the following digestion phases. Despite this, at the end of the intestinal phase, a portion of microparticles was still in the digestion medium.

Q-In-2% and Q-In-20% microparticles were subjected to inulinase at pH 6.8 to simulate the *in vitro* colonic digestion. The results showed that the greatest Q released occurred in the colonic phase, corresponding to the release of the encapsulated Q since the surface Q was released during the digestion phases that take place in the upper gastrointestinal tract. Inulinase degraded inulin by cleaving β-(2-1) linkage, allowing the encapsulated Q to be released in the colon. The Q released from amorphous microparticles at 18 h of colonic

digestion (Q-In-2%, 66.4 ± 2.5%, 27.6 ± 1.0 mg) was significantly higher than semicrystalline microparticles (Q-In-20%, 50.5 ± 2.1%, 20.9 ± 1.2 mg) (Figure 3). However, no significant differences were found between amorphous and semicrystalline microparticles for Q release at 24 h of colonic digestion (52.4 ± 3.2%, 21.8 ± 1.3 mg in Q-In-2% *vs*. 44.7 ± 2.6%, 18.5 ± 1.1mg in Q-In-20%). Quercetin content after 24 h of colonic digestion was lower than after 18 h, which may be attributed to quercetin degradation induced by the simulated colonic conditions (pH 6.8), involving the cleavage of the cinnamyl system (B- and C-rings) (Zhou & Sadik, 2008).

4. Conclusions

The strategy of blending inulin with inulin crystallite dispersions enables to obtain spray-dried quercetin-inulin microparticles with different CI, responding to the hypothesis. Both the percentage of inulin crystallite dispersion and the inlet air temperature influenced the CI of the microparticles, and the higher the percentage of inulin crystallite dispersion and the lower the inlet air temperature, the higher the CI values. Although inulin has the same structural features in all the microparticle systems, the different physical arrangement of inulin in amorphous and semicrystalline systems modifies its properties as encapsulating agent. Thus, the semicrystalline microparticle systems showed higher quercetin EE and hygroscopicity, as well as lower solubility, particle size and T_g than amorphous microparticles. The quercetin release during *in vitro* gastrointestinal digestion was not affected by the CI of the microparticles, and mainly the surface quercetin was released in all the microparticles systems, whereas encapsulated quercetin reached the colon where can exert its antioxidant and anti-inflammatory activity. In view of these results, the controlled crystallization in spray-dried microparticles opens a new start for the design of polyphenol-based microparticles with specific properties for the functional food industry.

Acknowledgments

The authors acknowledge to “Influencer Program 2022” of Anton Paar, Graz, Austria, in the period March to November 2022.

Funding

This research was supported by ANID (Fondecyt Project 1221038; National PhD Scholarship 21202543; Fondequip Project EQM 200266), Chile.

CRediT authorship contribution statement

Alejandra Quintriqueo-Cid: data curation, formal analysis, methodology, writing – original draft. Begoña Giménez: formal analysis, writing-original draft, writing – review & editing. Patricio Romero-Hasler: formal analysis, methodology, writing – original draft. Eduardo Soto-Bustamante: formal analysis, methodology, writing – original draft. Jesús Lozano-Sánchez: writing – review & editing. Paz Robert: conceptualization, project administration, funding acquisition, resources, supervision, writing – original draft, writing – review & editing.

Figure captions

Figure 1. Response surface graphs for crystallinity index when the independent variable (a) quercetin content, (b) inulin crystallite dispersion, and (c) inlet air temperature are in the middle value.

Figure 2. X-ray diffraction patterns for (a) quercetin-inulin (Q-In) microparticles, and (b) empty microparticles (In), both with three different crystallinity indexes (CI). Scanning electron microscopic photographs (magnification 6000X) for (c) Q-In-2% microparticles, (d) Q-In-12% microparticles, (e) Q-In-20% microparticles. Atomic Force Microscopy images for (f) Q-In-2% microparticles, (g) Q-In-20% microparticles at a 5x5 μm scan size, and (h) Q-In-20% at 1x1 μm scan size.

Figure 3. The release profile of quercetin from quercetin-inulin microparticles with three different crystallinity indexes (CI) under *in vitro* simulated digestion, and micrographs of the digestion process at the beginning and at the end of each phase (magnification 100X). Different letters (a – b) indicate significant differences ($p \leq 0.05$) among microparticle systems at the same digestion time. Q: Quercetin; In: Inulin; O: Oral; G: Gastric; I: Intestinal; C: Colon.

References

633 Ahmadian, Z., Niazmand, R., & Pourfarzad, A. (2019). Microencapsulation of saffron petal
634 phenolic extract: their characterization, *in vitro* gastrointestinal digestion, and storage
635 stability. *Journal of Food Science, 84*, 2745-2757. https://doi.org/10.1111/1750-3841.14807.
636
637 André, I., Mazeau, K., Tvaroska, I., Putaux, J.-L., Winter, W. T., Taravel, F. R., & Chanzy,
638 H. (1996). Molecular and crystal structures of inulin from electron diffraction data.
639 *Macromolecules, 29*, 4626-4635. https://doi.org/10.1021/ma951799f.
640
641 Ayala-Fuentes, J. C., Gallegos-Granados, M. Z., Villarreal-Gómez, L. J., Antunes-Ricardo,
642 M., Grande, D., & Chavez-Santoscoy, R. A. (2022). Optimization of the synthesis of natural
643 polymeric nanoparticles of inulin loaded with quercetin: characterization and cytotoxicity
644 effect. *Pharmaceutics, 14*, 888. https://doi.org/10.3390/pharmaceutics14050888.
645
646 Barclay, T. G., Rajapaksha, H., Thilagam, A., Qian, G., Ginic-Markovic, M., Cooper, P. D.,
647 Gerson, A., & Petrovsky, N. (2016). Physical characterization and in silico modeling of inulin
648 polymer conformation during vaccine adjuvant particle formation. *Carbohydrate Polymers*,
649 *143*, 108-115. https://doi.org/10.1016/j.carbpol.2016.01.062.
650
651 Boostani, S., & Jafari, S. M. (2021). A comprehensive review on the controlled release of
652 encapsulated food ingredients; fundamental concepts to design and applications. *Trends in*
653 *Food Science & Technology*, *109*, 303-321. https://doi.org/10.1016/j.tifs.2021.01.040.
654
655 Botrel, D. A., Rodrigues, I. C. B., de Souza, H. J. B., & Fernandes, R. V. de B. (2016).
656 Application of inulin in thin-layer drying process of araticum (*Annona crassiflora*) pulp.
657 *LWT – Food Science and Technology*, *69*, 32-39. https://doi.org/10.1016/j.lwt.2016.01.018.
658
659 Brodkorb, A., Egger, L., Alminger, M., Alvito, P., Assuncão, R., Ballance, S., Bohn, T.,
660 Bourlieu-Lacanal, C., Boutrou, R., Carrière, F., Clemente, A., Corredig, M., Dupont, D.,
661 Dufour, C., Edwards, C., Golding, M., Karakaya, S., Kirkhus, B., Le Feunteun, S., Lesmes,
662 U., Macierzanka, A., Mackie, A. R., Martins, C., Marze, S., McClements, D. J., Ménard, O.,
663 Minekus, M., Portmann, R., Santos, C. N., Souchon, I., Singh, R. P., Vegarud, G. E.,

Wickham, M. S. J., Weitschies, W., & Recio, I. (2019). INFOGEST static *in vitro* simulation of gastrointestinal food digestion. *Nature Protocols*, *14*, 991-1014. https://doi.org/10.1038/s41596-018-0119-1.

Cai, Y. Z., & Corke, H. (2000). Production and properties of spray-dried *amaranthus* betacyanin pigments. *Journal of Food Science*, *65*, 1248-1252. https://doi.org/10.1111/j.1365-2621.2000.tb10273.x.

Cano-Chauca, M., Stringheta, P. C., Ramos, A. M., & Cal-Vidal, J. (2005). Effect of the carriers on the microstructure of mango powder obtained by spray drying and its functional characterization. *Innovative Food Science and Emerging Technologies*, *6*, 420-428. https://doi.org/10.1016/j.ifset.2005.05.003.

Davidov-Pardo, G., Arozarena, I., & Marín-Arroyo, M. R. (2013). Optimization of a wall material formulation to microencapsulate a grape seed extract using a mixture design of experiments. *Food and Bioprocess Technology*, *6*, 941-951. https://doi.org/10.1007/s11947-012-0848-z.

Desai, N. M., Stanley, J. G., & Murthy, P. S. (2020). Green coffee nanoparticles: optimisation, *in vitro* bioactivity and bio-release property. *Journal of Microencapsulation*, *37*, 52-64. https//doi.org/10.1080/02652048.2019.1692946.

Estevinho, B. N., & Rocha, F. (2018). Application of biopolymers in microencapsulation processes. In A. M. Grumezescu, & A. M. Holban (Eds.), *Biopolymers for Food Design* (pp. 191-222). Academic Press. https://doi.org/10.1016/B978-0-12-811449-0.00007-

Gavini, E., Alamanni, M. C., Cossu, M., & Giunchedi, P. (2005). Tabletted microspheres containing Cynara scolymus (var. Spinoso sardo) extract for the preparation of controlled release nutraceutical matrices. *Journal of Microencapsulation*, *22*, 487-499. https://doi.org/10.1080/02652040500099919.

Glibowski, P., & Pikus, S. (2011). Amorphous and crystal inulin behavior in a water environment. *Carbohydrate Polymers*, *83*, 635-639. https://doi.org/10.1016/j.carbpol.2010.08.028.

Goëlo, V., Chaumun, M., Gonçalves, A., Estevinho, B. N., & Rocha, F. (2020). Polysaccharide-based delivery systems for curcumin and turmeric powder encapsulation using a spray-drying process. *Powder Technology*, *370*, 137-146. https://doi.org/10.1016/j.powtec.2020.05.016.

González, E., Gómez-Caravana, A. M., Giménez, B., Cebrián, R., Maqueda, M., Martínez-Férez, A., Segura-Carretero, A., & Robert, P. (2019). Evolution of the phenolic compounds profile of olive leaf extract encapsulated by spray-drying during *in vitro* gastrointestinal digestion. *Food Chemistry*, *279*, 40-48. https://doi.org/10.1016/j.foodchem.2018.11.127.

Hébette, C. L. M., Delcour, J. A., Koch, M. H. J., Booten, K., Kleppinger, R., Mischenko, N., & Reynaers, H. (1998). Complex melting of semi-crystalline chicory (*Cichorium intybus* L.) root inulin. *Carbohydrate Research*, *310*, 65-75. https://doi.org/10.1016/S0008-6215(98)00154-2

Herrmann, P. S. de P., Yoshida, C. M. P., Antunes, A. J., & Marcondes, J. A. (2004). Surface evaluation of whey protein films by atomic force microscopy and water vapour permeability analysis. *Packaging Technology and Science*, *17*, 267-273. https://doi.org/10.1002/pts.662.

Jain, A. K., Sood, V., Bora, M., Vasita, R., Katti, D. S. (2014). Electrosprayed inulin microparticles for microbiota triggered targeting of colon. *Carbohydrate Polymers*, *112*, 225-234. https://doi.org/10.1016/j.carbpol.2014.05.087.

Jantan, I., Haque, Md. A., Arshad, L., Harikrishnan, H., Septama, A. W., & Mohamed-Hussein, Z.-A. (2021). Dietary polyphenols suppress chronic inflammation by modulation of multiple inflammation-associated cell signaling pathways. *Journal of Nutritional Biochemistry*, *93*, 108634. https://doi.org/10.1016/j.jnutbio.2021.108634.

Karrar, E., Mahdi, A. A., Sheth, S., Ahmed, I. A. M., Manzoor, M. F., Wei, W., & Wang, X. (2021). Effect of maltodextrin combination with gum arabic and whey protein isolate on the microencapsulation of gurum seed oil using a spray-drying method. *International Journal of Biological Macromolecules, 171,* 208-216. https://doi.org/10.1016/j.ijbiomac.2020.12.045.

Kim, Y., Faqih, M. N., & Wang, S. S. (2001). Factors affecting gel formation of inulin. *Carbohydrate Polymers*, *46*, 135-145. https://doi.org/10.1016/S0144-8617(00)00296-4.

Mahdi, A. A., Mohammed, J. K., Al-Ansi, W., Ghaleb, A. D. S., Al-Maqtari, Q. A., Ma, M., Ahmed, M. I., & Wang, H. (2020). Microencapsulation of fingered citron extract with gum arabic, modified starch, whey protein, and maltodextrin using spray drying. *International Journal of Biological Macromolecules*, *152*, 1125-1134. https://doi.org/10.1016/j.ijbiomac.2019.10.201.

Mali, S., Grossmann, M. V. E., García, M. A., Martino, M. N., & Zaritzky, N. E. (2006). Effects of controlled storage on thermal, mechanical and barrier properties of plasticized films from different starch sources. *Journal of Food Engineering*, *75*, 453-460. https://doi.org/10.1016/j.jfoodeng.2005.04.031

Maqsoudlou, A., Mohebodini, H. & Jafari, S. M. (2020). Antioxidant activity analysis of nanoencapsulated food ingredients. In S. M. Jafari (Eds.), *Characterization of Nanoencapsulated Food Ingredients* (pp. 617-664). Academic Press. https://doi.org/10.1016/B978-0-12-815667-4.00018-.

Mensink, M. A., Frijlink, H. W., van der Voort Maarschalk, K., & Hinrichs, W. L. J. (2015). Inulin, a flexible oligosaccharide. II: Review of its pharmaceutical applications. *Carbohydrate Polymers*, *134*, 418-428. https://doi.org/10.1016/j.carbpol.2015.08.022.

Morelo, G., Giménez, B., Márquez-Ruiz, G., Holgado, F., Romero-Hasler, P., Soto-Bustamante, E., & Robert, P. (2019). Influence of the Physical State of Spray-Dried

Flavonoid-Inulin Microparticles on Oxidative Stability of Lipid Matrices. *Antioxidants, 8*, 520. https://doi.org/10.3390/antiox8110520.

Moreno, T., Cocero, M. J., & Rodríguez-Rojo, S. (2018). Storage stability and simulated gastrointestinal release of spray dried grape marc phenolics. *Food and Bioproducts Processing, 112*, 96-107. https://doi.org/10.1016/j.fbp.2018.08.011.

Palma, M., García, P., Márquez-Ruiz, G., Vergara, C., & Robert, P. (2014). Release kinetics of flavonoids in methyl linoleate from microparticles designed with inulin and channelizing agent. *Food Research International*, *64*, 99-105. https://doi.org/10.1016/j.foodres.2014.05.064.

Romano, N., Mobili, P., Zuñiga-Hansen, M. E., & Gómez-Zavaglia, A. (2018). Physico-chemical and structural properties of crystalline inulin explain the stability of *Lactobacillus plantarum* during spray-drying and storage. *Food Research International*, *113*, 167-174. https://doi.org/10.1016/j.foodres.2018.07.007.

Ronkart, S. N., Deroanne, C., Paquot, M., Fougnies, C., Lambrechts, J.-C., & Blecker, C. S. (2007). Characterization of the Physical State of Spray-Dried Inulin. *Food Biophysics, 2*, 83-92. https://doi.org/10.1007/s11483-007-9034-7.

Ronkart, S. N., Paquot, M., Blecker. C. S., Fougnies, C., Doran, L., Lambrechts, J. C., Norberg, B., & Deroanne, C. (2009a). Impact of the Crystallinity on the Physical Properties of Inulin during Water Sorption. *Food Biophysics, 4*, 49-58. https://doi.org/10.1007/s11483-008-9097-0.

Ronkart, S. N., Paquot, M., Fougnies, C., Deroanne, C., & Blecker, C. S. (2009b). Effect of water uptake on amorphous inulin properties. *Food Hydrocolloids, 23*, 922-927. https://doi.org/10.1016/j.foodhyd.2008.06.003.

Ruiz Canizales, J., Basilio Heredia, J., Domínguez Avila, J., Madera Santana, T. J., Villegas Ochoa, M. A., Robles Sánchez, R. M., & González Aguilar, G. A. (2019). Microencapsulation of blue maize (*Zea mays* L.) polyphenols in two matrices: their stability during storage and *in vitro* digestion release. *Journal of Food Measurement and Characterization*, *13*, 892-900. https://doi.org/10.1007/s11694-018-0003-2.

Srinivas, K., King, J. W., Howard, L. R., & Monrad, J. K. (2010). Solubility and solution thermodynamic properties of quercetin and quercetin dihydrate in subcritical water. *Journal of Food Engineering*, *100*, 208-218. https://doi.org/10.1016/j.jfoodeng.2010.04.001.

Sun-Waterhouse, D., Wadhwa, S. S., & Waterhouse, G. I. N. (2013). Spray-Drying microencapsulation of polyphenol bioactives: a comparative study using different natural fibre polymers as encapsulants. *Food and Bioprocess Technology*, *6*, 2376-2388. https://doi.org/10.1007/s11947-012-0946-y.

Zhou, A., & Sadik, O. A. (2008). Comparative analysis of quercetin oxidation by electrochemical, enzymatic, autoxidation, and free radical generation techniques: a mechanistic study. *Journal of Agricultural and Food Chemistry*, *56*, 12081-12091. https://doi.org/10.1021/jf802413v.

Table 1. Statistical Box Behnken design applied for the microencapsulation of quercetin in blends of inulin and inulin crystallite dispersions by spray drying, and analysis of variance (ANOVA) for crystallinity index.

Inlet air temperature (°C)	Inulin crystallite dispersion (%)	Quercetin content (g)	Crystallinity index (%)
120	0	0.35	4.6 ± 0.5
200	0	0.35	2.1 ± 0.3
120	100	0.35	20.1 ± 0.8
200	100	0.35	3.4 ± 0.3
120	50	0.2	12.1 ± 1.3
200	50	0.2	2.9 ± 0.5
120	50	0.5	15.0 ± 0.3
200	50	0.5	2.6 ± 0.1
160	0	0.2	2.2 ± 0.4
160	100	0.2	17.2 ± 0.1
160	0	0.5	3.4 ± 0.3
160	100	0.5	13.6 ± 0.5
160	50	0.35	13.3 ± 2.1
160	50	0.35	11.3 ± 1.4
160	50	0.35	10.6 ± 0.3

Effect	Estimate	*p*-value
Average	8.96	
Inlet air temperature	-10.20	0.0093*
Inulin crystallite dispersion	10.50	0.0088*
Quercetin content	0.05	0.9643
Inlet air temperature x Inulin crystallite dispersion	-7,10	0.0368*
Lack-of-fit		0.2421
R^2 (%)	89.1	
R^2 adjusted for degrees of freedom (%)	84.7	

*: significant ($p \leq 0.05$).

Table 2. Characterization of quercetin-inulin microparticles with three different crystallinity indexes.

Parameters	**Q-In-2%**	**Q-In-12%**	**Q-In-20%**
Infeed formulation and spray-dryer operation conditions			
Inlet air temperature (°C)	200	160	120
Inulin crystallite dispersion (%)	0	50	100
Quercetin content (g)	0.35	0.35	0.35
Characterization of quercetin-inulin microparticles			
Quercetin content (mg/g microparticles)	32.00 ± 0.06	31.92 ± 0.18	30.95 ± 0.41
CI (%)	2.0 ± 0.28^{c}	12.0 ± 1.40^{b}	20.0 ± 0.85^{a}
EE (%)	70.5 ± 0.4^{c}	72.1 ± 0.3^{b}	76.4 ± 0.3^{a}
Particle size ($D_{4,3}$) (μm)	7.15 ± 0.66^{a}	6.52 ± 0.75^{a}	5.74 ± 0.78^{a}
Recovery (%)	94.7 ± 0.2^{a}	91.5 ± 0.4^{b}	94.4 ± 0.6^{a}
Moisture (%)	2.29 ± 0.07^{b}	2.56 ± 0.04^{ab}	2.84 ± 0.27^{a}
Hygroscopicity (g/100 g)	17.60 ± 0.57^{b}	24.77 ± 2.76^{ab}	29.50 ± 2.55^{a}
Solubility (%)	85.2 ± 1.0^{a}	75.6 ± 1.8^{b}	52.1 ± 0.8^{c}
Water activity	0.256 ± 0.010^{a}	0.205 ± 0.012^{b}	0.206 ± 0.005^{b}

Q: Quercetin; In: Inulin; CI: Crystallinity index, EE: Encapsulation efficiency. Different letters (a – c) in the same raw indicate significant differences ($p \leq 0.05$) among microparticles.

Table 3. Thermal properties of quercetin-inulin (Q-In) microparticles and empty microparticles (In) with three different crystallinity indexes.

	Q-In-2%	Q-In-12%	Q-In-20%	In-2%	In-12%	In-20%
T_g (°C)	85.45 ± 3.32^{a}	75.55 ± 2.90^{ab}	64.55 ± 2.05^{bc}	74.85 ± 1.20^{ab}	74.15 ± 0.21^{abc}	62.90 ± 5.37^{c}
T_c (°C)	136.10 ± 4.53^{a}	104.15 ± 2.76^{b}	84.25 ± 4.17^{c}	126.50 ± 1.98^{a}	100.05 ± 0.07^{b}	83.85 ± 3.75^{c}
ΔH_c (J/g)	-16.90 ± 4.24^{c}	-18.60 ± 0.14^{b}	-5.40 ± 0.00^{a}	-25.80 ± 1.70^{b}	-16.85 ± 0.35^{bc}	-3.40 ± 0.71^{a}
T_{m1} (°C)	-	-	136.30 ± 1.12	-	-	-
ΔH_{m1} (J/g)	-	-	1.26 ± 0.01	-	-	-
T_{m2} (°C)	-	161.10 ± 1.13^{a}	146.15 ± 0.50^{c}	-	156.15 ± 0.07^{b}	149.65 ± 1.34^{c}
ΔH_{m2} (J/g)	-	2.55 ± 0.21^{a}	4.00 ± 0.42^{a}	-	3.05 ± 0.07^{a}	3.70 ± 0.57^{a}
T_{m3} (°C)	168.90 ± 1.27^{a}	169.70 ± 0.57^{a}	163.65 ± 0.64^{b}	171.20 ± 0.71^{a}	169.10 ± 0.14^{a}	161.85 ± 0.64^{b}
ΔH_{m3} (J/g)	22.80 ± 6.79^{b}	38.05 ± 3.89^{a}	36.90 ± 1.27^{ab}	49.65 ± 4.03^{a}	40.45 ± 0.21^{a}	35.25 ± 0.21^{ab}
T_d (°C)	198.70 ± 1.84^{a}	198.95 ± 1.34^{a}	192.85 ± 1.63^{c}	198.10 ± 0.71^{ab}	195.60 ± 0.85^{abc}	193.50 ± 0.28^{bc}
ΔH_d (J/g)	154.95 ± 18.74^{a}	176.00 ± 2.97^{a}	179.95 ± 2.76^{a}	143.25 ± 0.21^{a}	149.10 ± 9.05^{a}	178.15 ± 14.35^{a}

Q: Quercetin; In: Inulin; T_g: Glass transition temperature; T_c: Crystallization temperature; ΔH_c: Crystallization enthalpy; T_{m1}: Melting temperature for the first melting transition; ΔH_{m1}: Enthalpy for the first melting transition; T_{m2}: Melting temperature for the second melting transition; ΔH_{m2}: Enthalpy for the second melting transition; T_{m3}: Melting temperature for the third melting transition; ΔH_{m3}: Enthalpy for the third melting transition; T_d: Degradation temperature; ΔH_d: Degradation enthalpy. Different letters (a – c) in the same row indicate significant differences ($p \leq 0.05$) among microparticles.

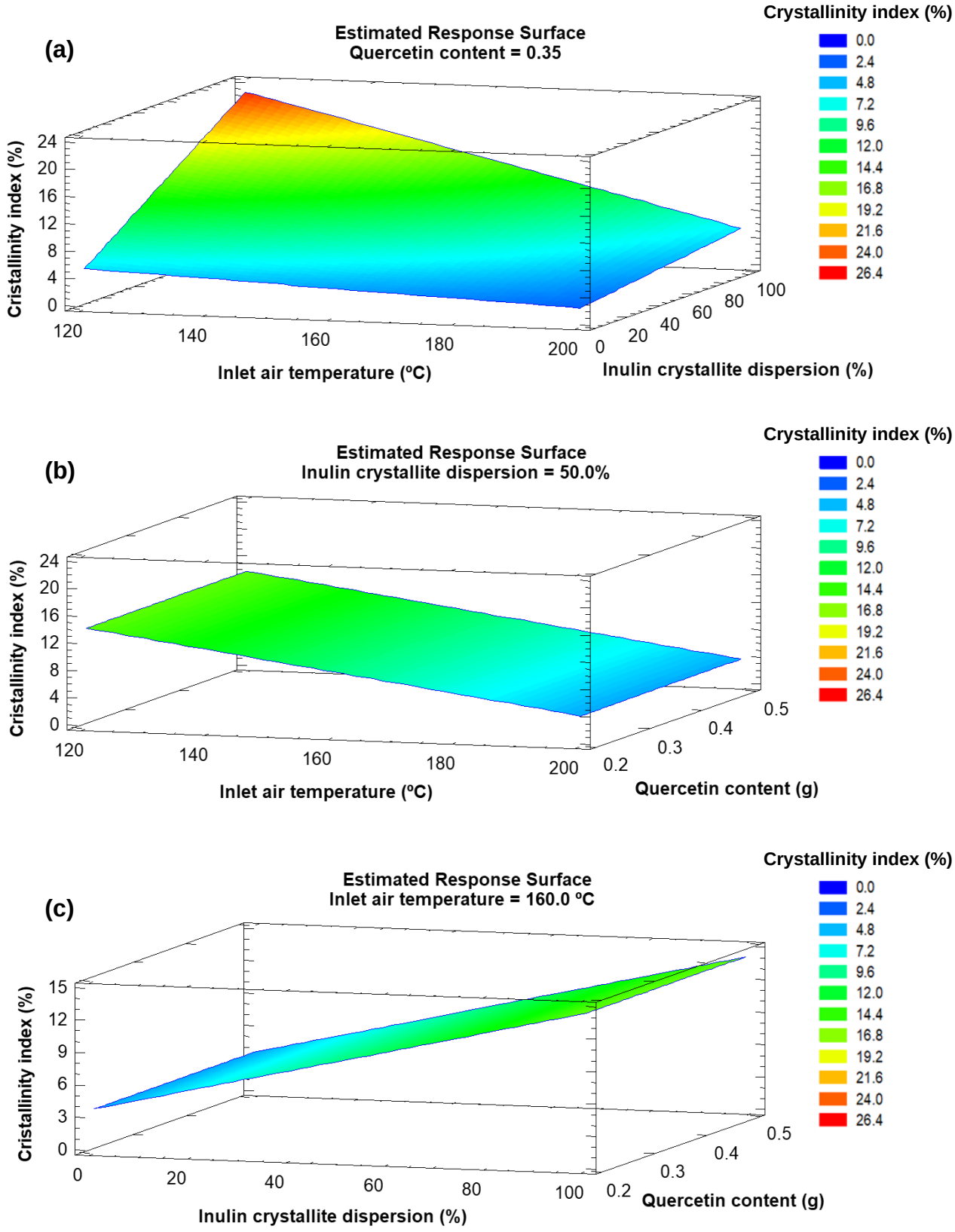
(a)
Estimated Response Surface
Quercetin content = 0.35
Crystallinity index (%)
0.0
2.4
4.8
7.2
9.6
12.0
14.4
16.8
19.2
21.6
24.0
26.4
Cristallinity index (%)
0
4
8
12
16
20
24
120
140
160
180
200
Inlet air temperature (ºC)
0
20
40
60
80
100
Inulin crystallite dispersion (%)
(b)
Estimated Response Surface
Inulin crystallite dispersion = 50.0%
Crystallinity index (%)
Cristallinity index (%)
Inlet air temperature (ºC)
0.2
0.3
0.4
0.5
Quercetin content (g)
(c)
Estimated Response Surface
Inlet air temperature = 160.0 ºC
Crystallinity index (%)
Cristallinity index (%)
0
3
6
9
12
15
Inulin crystallite dispersion (%)
Quercetin content (g)

Figure 1

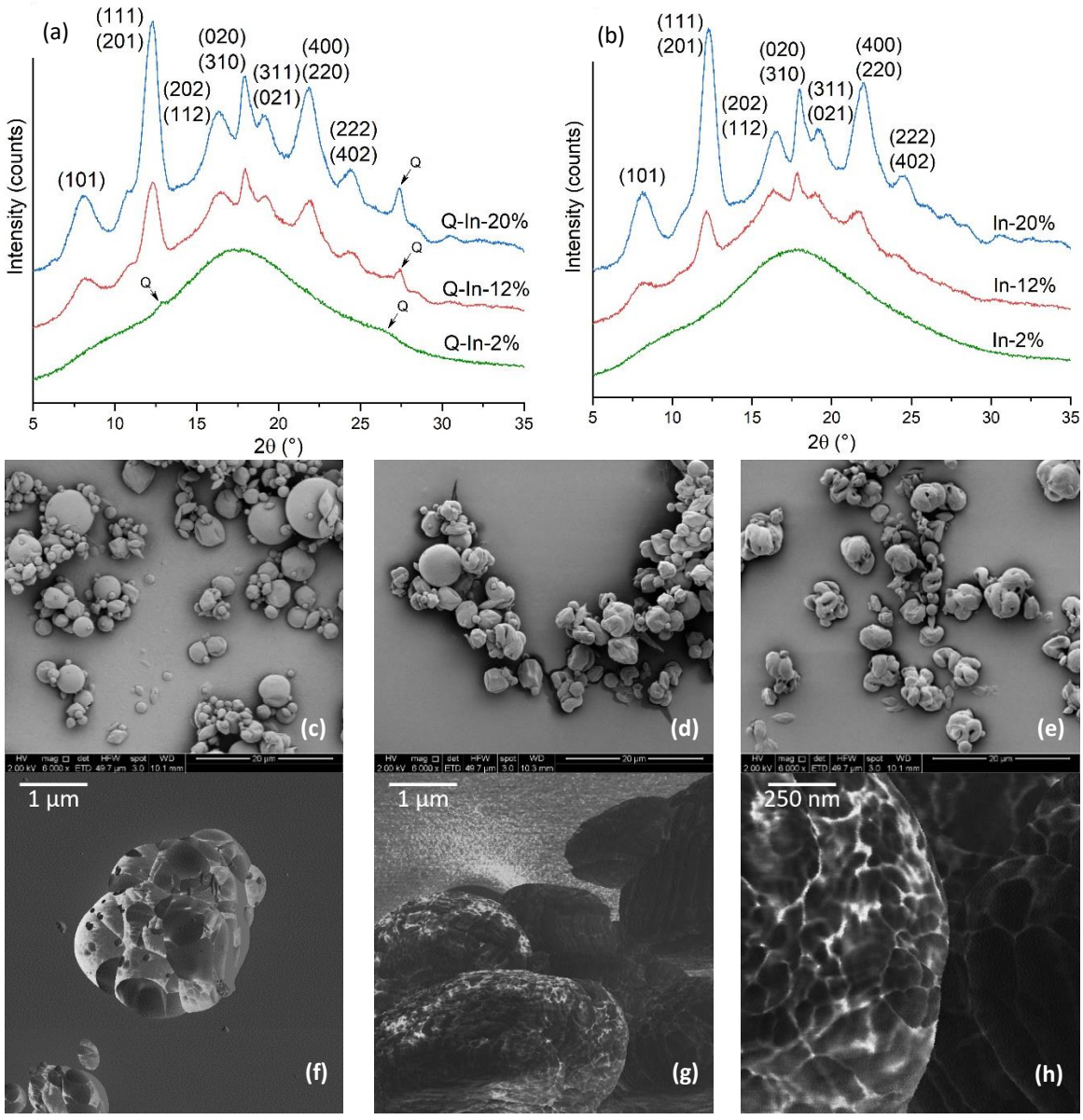
(a)
(111)
(201)
(020)
(310)
(400)
(220)
(202)
(112)
(311)
(021)
(222)
(402)
(101)
Q
Q-In-20%
Q-In-12%
Q-In-2%
Intensity (counts)
2θ (°)
(b)
In-20%
In-12%
In-2%
(c)
(d)
(e)
1 µm
1 µm
250 nm
(f)
(g)
(h)

Figure 2

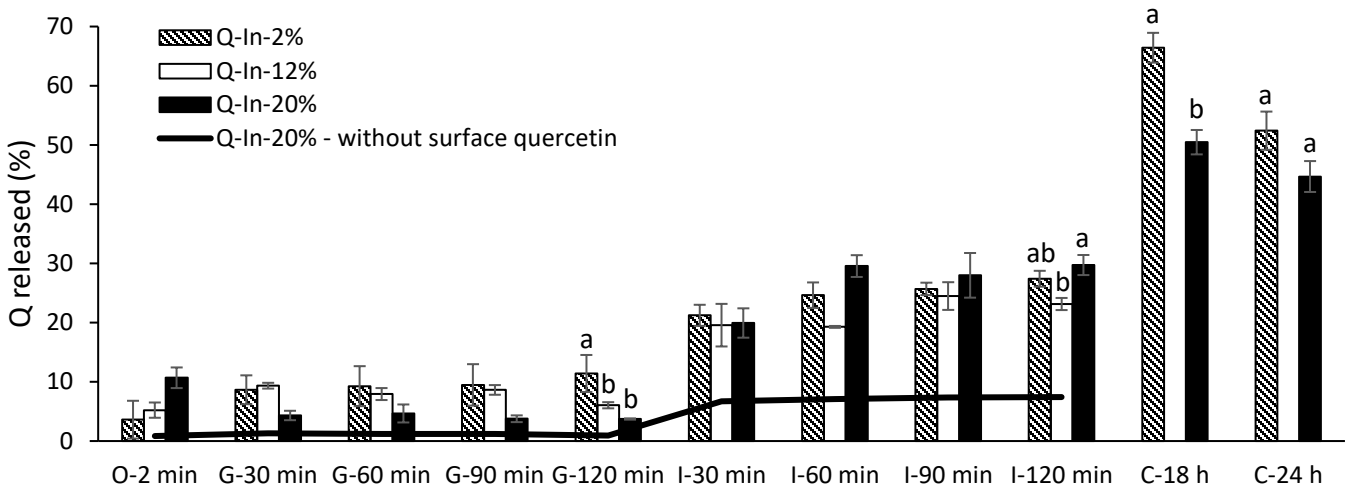
Q-In-2%
Q-In-12%
Q-In-20%
Q-In-20% - without surface quercetin
Q released (%)
70
60
50
40
30
20
10
0
a
b
b
ab
b
a
a
b
a
O-2 min
G-30 min
G-60 min
G-90 min
G-120 min
I-30 min
I-60 min
I-90 min
I-120 min
C-18 h
C-24 h

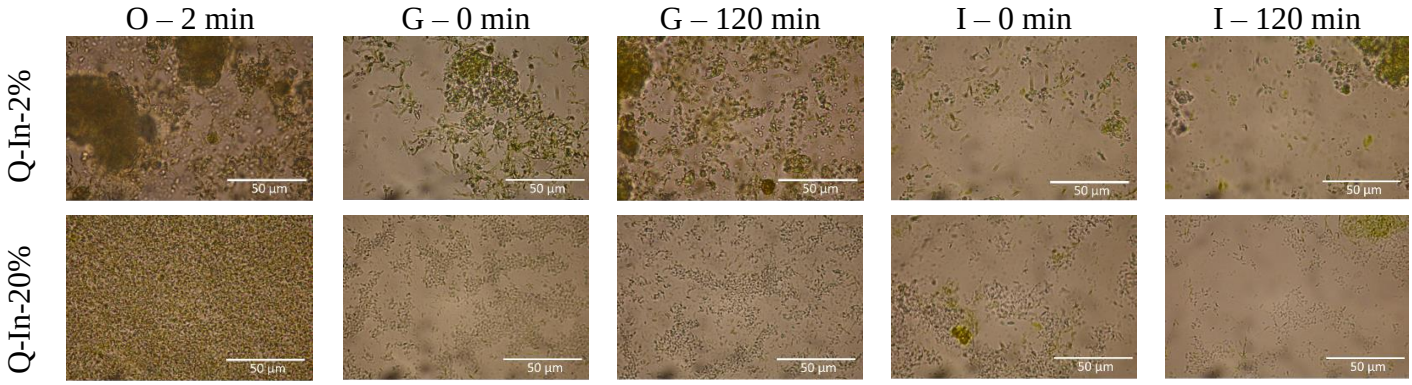
O – 2 min
G – 0 min
G – 120 min
I – 0 min
I – 120 min
Q-In-2%
Q-In-20%
50 µm

Figure 3

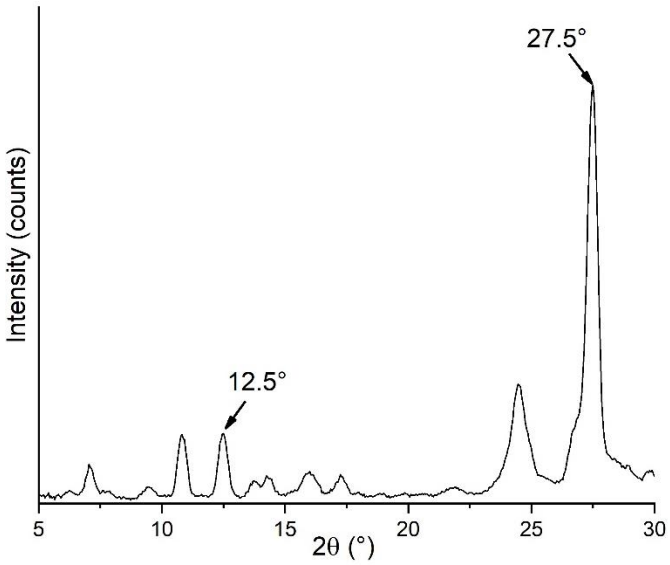

Figure S1. X-ray diffraction pattern for quercetin.

(a)

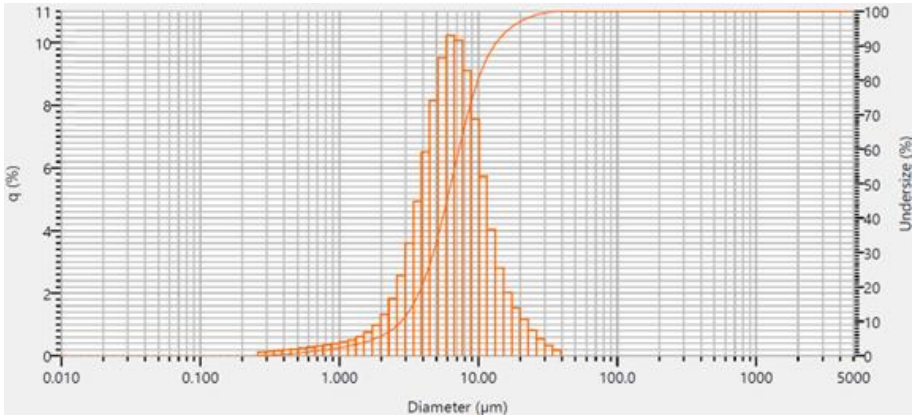

(b)

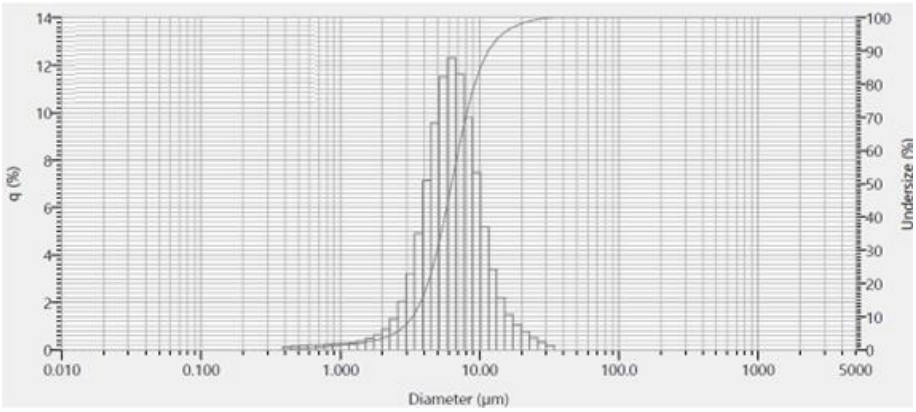

(c)

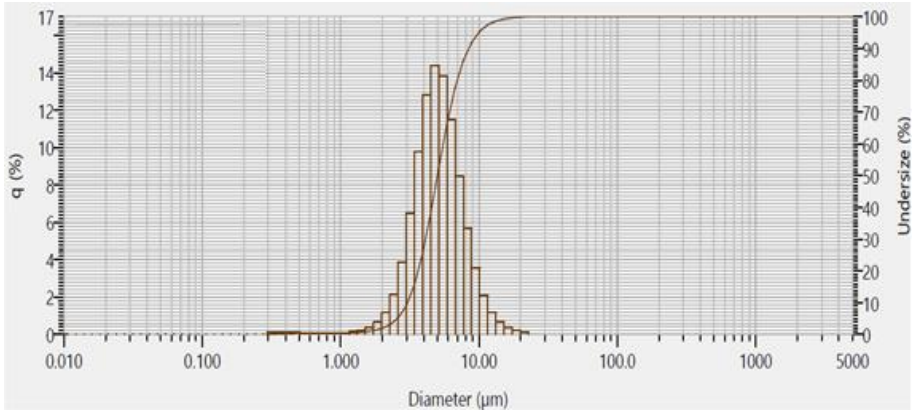

Figure S2. Particle size distribution for (a) Q-In-2% microparticles, (b) Q-In-12% microparticles, (c) Q-In-20% microparticles.

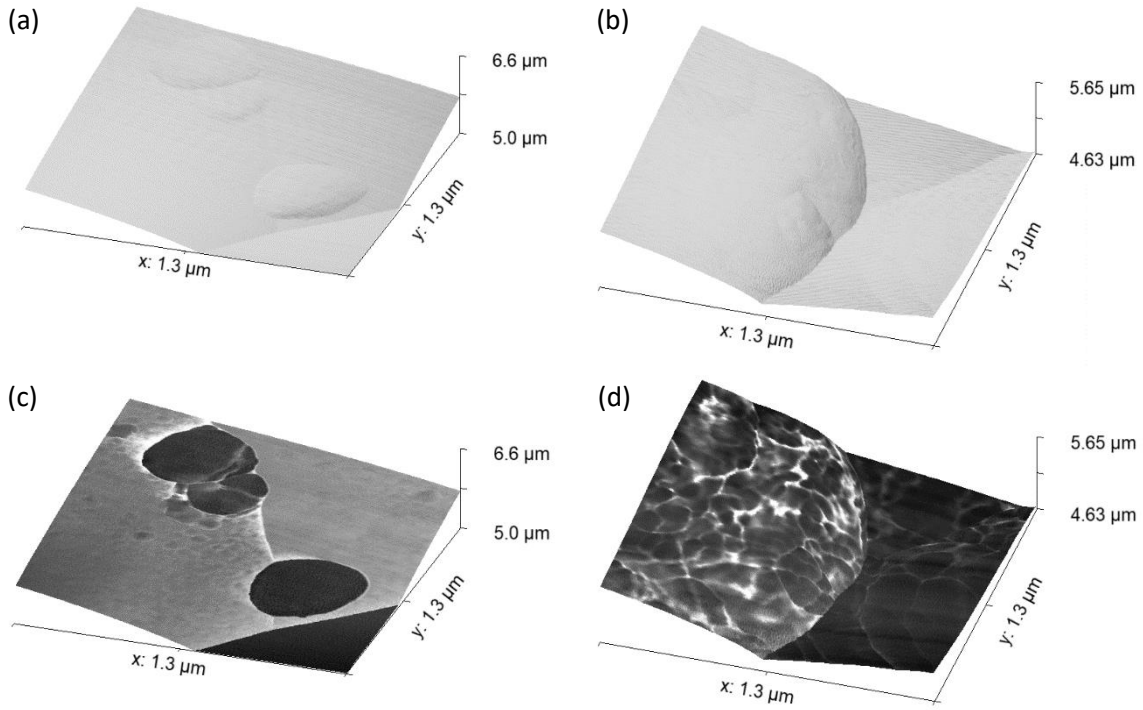

Figure S3. 3D images of a) Q-In-2% microparticles and b) Q-In-20% showing the surface topology. Composite 3D images of c) Q-In-2% microparticles and d) Q-In-20% using the phase information as shading, showing the contrast in composition for both microparticles.

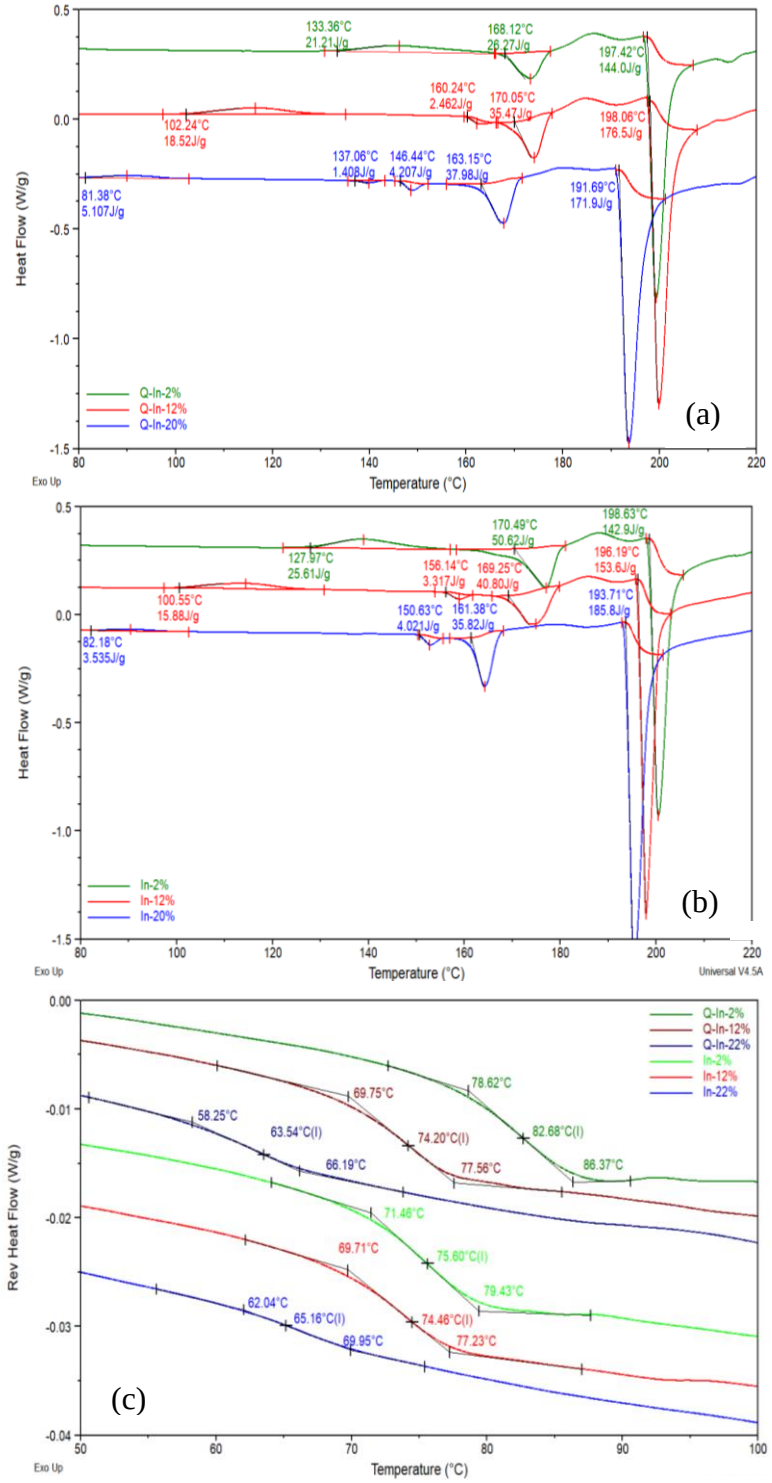

Figure S4. Thermal properties: (a) recrystallization, melting, and degradation behavior for quercetin-inulin (Q-In) microparticles with three different crystallinity indexes (CI), (b) recrystallization, melting, and degradation behavior for empty (In) microparticles with three different CI, (c) glass transition temperatures (T_g) determined from reversible heat flow thermograms for empty (In) and Q-In microparticles with three different CI.